Radiation and Scattering from Ferrite-Tuned Cavity-Backed Slot Antennas: Theory and Experiment

Anastasis C. Polycarpou, *Student Member, IEEE,* Constantine A. Balanis, *Fellow, IEEE,* James T. Aberle, *Senior Member, IEEE,* and Craig Birtcher

***Abstract*— A three-dimensional finite-element method hybridized with the spectral/spatial domain method of moments is presented for the analysis of ferrite-tuned cavity-backed slot antennas. The cavity, which is partially filled with magnetized ferrite layers, is flush mounted on an infinite ground plane with possible dielectric or magnetic overlay. The antenna operates primarily in the ultrahigh-frequency band. The finite-element method is used to solve for the electric-field distribution inside the cavity, whereas the spectral-domain approach is used to solve for the exterior region. An asymptotic extraction of the exponential behavior of the Green's function followed by a spatial evaluation of the resulting integral is used to improve computational speed. Radar cross section, input impedance, return loss, gain, and efficiency of ferrite-tuned cavity-backed slots (CBS) are calculated for various biasing conditions. Numerical results are compared with experimental data.**

***Index Terms*—Ferrites, hybrid methods, slot antennas.**

I. Introduction

FERRITES have been used for many years in microwave and millimeter-wave devices such as circulators, isolators, switches, and phase shifters [1]. The material properties of ferrites are controlled by the direction and strength of an externally applied magnetic field. This unique property of ferrimagnetic materials has found applications not only in microwave integrated circuits (MIC's), but also in antenna technology [2]–[9]. The use of magnetized ferrites in antenna design provides desirable features such as tunability, polarization diversity, beam steering, radar cross-section (RCS) control, surface wave reduction, and gain enhancement.

Although magnetized ferrites have been extensively used to enhance antenna characteristics through altering the bias field, most of previous work was concentrated mainly on RCS evaluation of printed dipoles and microstrip patch antennas. The resonant behavior of the antenna element has been thoroughly investigated for various biasing conditions. An important conclusion from these studies is that the bias field strongly affects the resonant frequency of all modes with dominant electric field in the direction of magnetization. An excellent study on radiation characteristics of patch antennas printed on normally biased ferrite substrates was originally performed by Pozar [4], [5]. Numerous results were presented illustrating the effect of biasing on antenna efficiency, resonant frequency and input impedance. Using a similar approach, Yang [6], [7] examined the effects of arbitrary magnetization on the RCS response of microstrip patches on ferrite substrates. He also used ferrite superstrates for the design of switchable antennas. Another similar study was recently published by Lee *et al.* [8] using in-plane biased ferrite substrates. RCS comparisons between the magnetized and unmagnetized cases were presented. Analysis of infinite dipole arrays printed on ferrite substrates was carried out by Buris *et al.* [9]. Emphasis was concentrated primarily on scan performance and input impedance calculations.

In this paper, ferrites are used as loading materials inside a cavity-backed slot (CBS) mounted on an infinite ground plane. The CBS is considered both as a scatterer and as a radiator. Unlike previous work on microstrip antennas using ferrite substrates, the current study is primarily focused on operating the CBS in the ultrahigh-frequency (UHF) band rather than the microwave band. The cavity, which was chosen to be square, is excited using a cylindrical probe in a direction parallel to the ground plane. A dc magnetic field is applied in the direction of the probe, although other directions of magnetization may be considered. The first mode that is excited inside the cavity is the TE_{10}, which exhibits a dominant electric field in the direction of the probe. Since the magnetization is oriented in the direction of the dominant electric field, the resonant frequency of the TE_{10} mode is expected to shift if the strength of the bias field is altered. This type of mode is sometimes referred to as a magnetostatic mode attributed to the presence of a strong extraordinary wave inside the ferrite sample. In the absence of the bias field, the resonance due to the magnetostatic mode totally disappears. This property of ferrites is often utilized in the design of switchable antennas [7].

A vector finite-element method (FEM) hybridized with the method of moments (MoM) is used in the analysis of ferrite-loaded CBS antennas. The FEM, which is based on linear tetrahedral elements, solves for the electric field distribution inside the cavity. A spectral-domain MoM is implemented through the continuity of the tangential magnetic field in the aperture to solve for the field distribution in the exterior region; note that the cavity is mounted on an infinite ground plane with a possible dielectric/magnetic overlay. The main drawback of the spectral-domain MoM is that it becomes extremely slow with increasing the number of edges in the aperture. This problem is overcome by using an asymptotic

Manuscript received October 2, 1997; revised June 12, 1998. This work was supported by the Advanced Helicopter Electromagnetics Industrial Associates Program and NASA Grant NAG-1-1082.

The authors are with the Department of Electrical Engineering, Telecommunications Research Center, Arizona State University, Tempe, AZ 85287 USA.

Publisher Item Identifier S 0018-926X(98)07053-7.

extraction of the exponential behavior of the Green's function; the asymptotic part is evaluated using a computationally efficient spatial-domain integration. The excitation is based on either a plane wave incidence or a coaxial feed model implemented using the FEM. RCS, input impedance, return loss, and gain versus frequency are calculated using the hybrid formulation. Parametric studies in terms of bias field, linewidth, and saturation magnetization are also performed. Numerical results are compared with a pure spectral-domain MoM formulated independently by Kokotoff [10] as well as experimental data. All experiments were performed in the anechoic chamber of Arizona State University using an HP8510 network analyzer. Comparisons between predictions and measurements illustrate excellent agreement.

II. Analysis

A. FEM/MoM Formulation

A two-dimensional (2-D) view of a ferrite-loaded CBS antenna mounted on an infinite ground plane coated with a dielectric layer is depicted in Fig. 1. A vector FEM is implemented for the solution of the source-free Helmholtz's equation

$$\nabla \times \left([\mu_r]^{-1} \cdot \nabla \times \mathbf{E}\right) - k_\circ^2 [\epsilon_r]\mathbf{E} = 0 \tag{1}$$

inside the cavity volume (Ω), where $[\epsilon_r]$ and $[\mu_r]$ are, respectively, the permittivity and permeability tensors of the domain and $\mathbf{E}$ is the unknown electric field. Full-tensor representation of ϵ_r and μ_r allows electromagnetic modeling of frequency-dependent anisotropic materials. Dirichlet boundary conditions are imposed on all perfectly conducting surfaces, which implies that $\hat{n} \times \mathbf{E} = 0$ on cavity walls. Using this boundary condition and the well-known Galerkin's approach, the Helmholtz's equation can be written in a weak integral form given by

$$\begin{aligned} &\iiint_\Omega ([\mu_r]^{-1} \nabla \times \mathbf{E}) \cdot (\nabla \times \mathbf{W})\, dV \\ &\quad - k_\circ^2 \iiint_\Omega [\epsilon_r] \cdot \mathbf{E} \cdot \mathbf{W}\, dV \\ &\quad + jk_\circ \eta_\circ \iint_S \mathbf{H} \cdot (\mathbf{W} \times \hat{a}_z)\, dA = 0 \end{aligned} \tag{2}$$

where $\mathbf{W}$ is the chosen testing function, $k_\circ$ is the free-space propagation constant, $\eta_\circ$ is the free-space intrinsic impedance, and S denotes the area of the cavity aperture.

For scattering, a linearly polarized plane wave (denoted by $\mathbf{H}^{inc}$) is incident on the aperture plane at an angle θ_i with respect to the normal vector and ϕ_i with respect to the x axis. By imposing the boundary condition that the tangential magnetic field must be continuous across the aperture plane, one may write

$$\begin{aligned} \mathbf{H} = \mathbf{H}^{inc} + \mathbf{H}^{ref} + \frac{1}{4\pi^2} \iint_{-\infty}^{\infty} \widetilde{\mathbf{M}}(k_x, k_y) \\ \cdot \overline{\overline{\widetilde{\mathbf{G}}}}(k_x, k_y, z|0) e^{j(k_x x + k_y y)}\, dk_x\, dk_y \end{aligned} \tag{3}$$

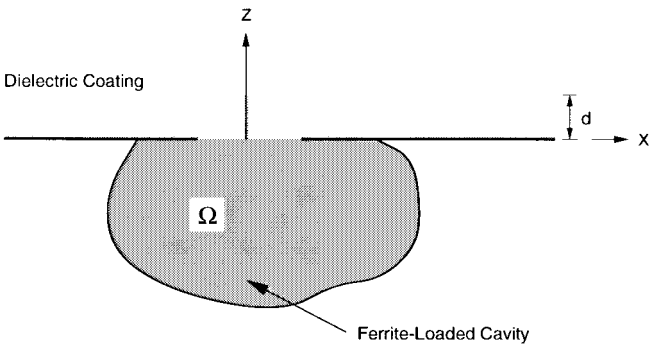

Fig. 1. Two-dimensional view of a ferrite-loaded CBS.

where $\mathbf{H}^{ref}$ is the magnetic field reflected by the coated ground plane in the absence of the aperture, $\overline{\overline{\widetilde{\mathbf{G}}}}$ is the spectral dyadic Green's function for a coated conducting ground plane in the presence of a magnetic current source at the origin and $\widetilde{\mathbf{M}}$ is the Fourier transform of the magnetic current ($\mathbf{E} \times \hat{a}_z$) just above the aperture. Substituting (3) into (2) and utilizing the inverse Fourier transform in conjunction with the definition that $\mathbf{T} = \mathbf{W} \times \hat{a}_z$, the weak form of Helmholtz's equation can be expressed as

$$\begin{aligned} &\iiint_\Omega ([\mu_r]^{-1} \nabla \times \mathbf{E}) \cdot (\nabla \times \mathbf{W})\, d\Omega \\ &\quad - k_\circ^2 \iiint_\Omega [\epsilon_r]\mathbf{E} \cdot \mathbf{W}\, d\Omega - \frac{jk_\circ \eta_\circ}{4\pi^2} \iint_{-\infty}^{\infty} \\ &\quad \cdot \widetilde{\mathbf{M}}(k_x, k_y) \cdot \overline{\overline{\widetilde{\mathbf{G}}}}(k_x, k_y, z|0) \cdot \widetilde{\mathbf{T}}(-k_x, -k_y)\, dk_x\, dk_y \\ &= jk_\circ \eta_\circ \iint_S (\mathbf{H}_{\tan}^{inc} + \mathbf{H}_{\tan}^{ref}) \cdot \mathbf{T}\, dA. \end{aligned} \tag{4}$$

The finite-element volume is discretized with tetrahedrons and the aperture with triangles. Thus, the electric field ($\mathbf{E}$) inside the cavity is expanded in terms of a set of basis functions $\mathbf{W}_i$'s and the magnetic current ($\mathbf{M}$) in the aperture is expanded in terms of another set of basis functions $\mathbf{T}_i$'s, where i corresponds to a global edge number. The second type of basis functions ($\mathbf{T}_i$'s) were originally proposed by Rao *et al.* [11]. These are very similar to $\mathbf{W}_i$'s with the only difference being the enforcement of normal continuity rather than tangential continuity across edges. The Fourier transform of these triangular basis functions is known in closed form [12].

The integral on the right-hand side of (4) represents the excitation vector, which is evaluated using a pure spectral-domain approach. The spectral integral on the left-hand side of (4) represents the admittance matrix for the exterior region of the cavity. The latter is evaluated using a mixed spectral/spatial-domain MoM approach. The exponential behavior of the governing Green's function is numerically extracted to improve the computational speed of the spectral integration. The asymptotic part is evaluated using a spatial integration, which is known to be computationally more efficient. Thus, using the asymptotic extraction, the admittance matrix can be expressed

in spectral domain as

$$Y_{ij} = -\frac{jk_\circ\eta_\circ}{4\pi^2}\iint_{-\infty}^{\infty}\widetilde{\mathbf{T}}_i(k_x,k_y)\cdot\left\{\overline{\overline{\widetilde{\mathbf{G}}}}(k_x,k_y,z|0)-\overline{\overline{\widetilde{\mathbf{G}}}}_h(k_x,k_y,z|0)\right\}\cdot\widetilde{\mathbf{T}}_j(-k_x,-k_y)\,dk_x\,dk_y - \frac{jk_\circ\eta_\circ}{4\pi^2}\int\int_{-\infty}^{\infty}\widetilde{\mathbf{T}}_i(k_x,k_y)\cdot\overline{\overline{\widetilde{\mathbf{G}}}}_h(k_x,k_y,z|0)\cdot\widetilde{\mathbf{T}}_j(-k_x,-k_y)\,dk_x\,dk_y \tag{5}$$

where $\overline{\overline{\widetilde{\mathbf{G}}}}_h$ is the dyadic Green's function of a homogeneous space with $\epsilon_r = \epsilon_r^d$ and $\mu_r = \mu_r^d$ (ϵ_r^d and μ_r^d referred to the dielectric coating), and $\widetilde{\mathbf{T}}_i$ is the Fourier transform of the ith basis function. The first integral in (5) denoted as $\widetilde{Y}_{ij}$ is evaluated using a pure spectral-domain approach after converting to polar coordinates. The second integral in (5), denoted as Y_{ij}^H, is evaluated using a spatial instead of spectral domain MoM

$$Y_{ij}^H = -2k^2\int_{A_i}\mathbf{T}_i(\mathbf{r})\cdot\left[\int_{Aj}\mathbf{T}_j(\mathbf{r}')\,G_h(\mathbf{r},\mathbf{r}')\,dA'\right]dA + 2\int_{A_i}\nabla\cdot\mathbf{T}_i(\mathbf{r})\left[\int_{A_j}G_h(\mathbf{r},\mathbf{r}')\nabla'\cdot\mathbf{T}_j(\mathbf{r}')\,dA'\right]dA \tag{6}$$

where A_i (A_j) is the triangle supporting the ith (jth) basis function, $\mathbf{r}$ ($\mathbf{r}'$) is the position vector, and G_h is the Green's function for a homogeneous medium with $\epsilon_r = \epsilon_r^d$, and $\mu_r = \mu_r^d$.

Once the unknowns (non-PEC edges) inside the cavity and aperture are assembled, a linear system of equations is formed

$$\begin{bmatrix}M^{c/c} & M^{c/a}\\ M^{a/c} & M^{a/a}+Y^{a/a}\end{bmatrix}\begin{bmatrix}E^c\\E^a\end{bmatrix}=\begin{bmatrix}0\\b^a\end{bmatrix}$$

where $[M]$ represents the finite-element matrix given by

$$M_{ij} = \iiint_\Omega(\nabla\times\mathbf{W}_i)\cdot[\mu_r]^{-1}\cdot(\nabla\times\mathbf{W}_j)\,d\Omega - k_\circ^2\iiint_\Omega\mathbf{W}_i\cdot[\epsilon_r]\cdot\mathbf{W}_j\,d\Omega \tag{7}$$

and $[Y]=[\widetilde{Y}]+[Y^H]$; the superscripts c and a, which denote cavity and aperture, respectively, are used to distinguish field interactions between the two regions. The rank of matrix $[M]$ is N_c+N_a where N_c is the number of non-PEC edges inside the cavity and N_a is the number of non-PEC edges in the aperture. The rank of matrix $[Y]$ is N_a.

The right-hand-side vector, which is nonzero only in the aperture plane and expressed by the surface integral in (4), can be evaluated very conveniently using the spectral-domain approach

$$b_i^a(hard) = \frac{2}{\eta_\circ}\widetilde{G}_\theta^M(k_{xs},k_{ys})\cos\theta_i\cdot e^{jk_\circ d\cos\theta_i}\left\{\widetilde{T}_{xi}^*(k_{xs},k_{ys})\sin\phi_i-\widetilde{T}_{yi}^*(k_{xs},k_{ys})\cos\phi_i\right\} \tag{8}$$

$$b_i^a(soft) = \frac{2}{\eta_\circ}\widetilde{G}_\phi^M(k_{xs},k_{ys})\cos\theta_i\cdot e^{jk_\circ d\cos\theta_i}\left\{\widetilde{T}_{xi}^*(k_{xs},k_{ys})\cos\phi_i+\widetilde{T}_{yi}^*(k_{xs},k_{ys})\sin\phi_i\right\} \tag{9}$$

for hard and soft polarization, respectively; i denotes the global number of an edge in the aperture, * indicates complex conjugate, and

$$k_{xs} = k_\circ\sin\theta_i\cos\phi_i \qquad k_{ys} = k_\circ\sin\theta_i\sin\phi_i. \tag{10}$$

The Green's function definitions for $\widetilde{G}_\theta^M$ and $\widetilde{G}_\phi^M$ as well as additional details in the derivation of (8) and (9) are provided in [13] and [14].

For radiation, the formulation remains the same except for the excitation vector which is formulated in a different way. Instead of plane wave incidence, the antenna is now excited using a coaxial feed model that becomes part of the finite-element domain. The associated formulation for the coaxial feed model and the evaluation of the reflection coefficient at the coax/cavity interface are explicitly given in [13].

The far-zone radiated and/or scattered fields are calculated using the magnetic current distribution in the aperture. Specifically, these are given by

$$E_\theta = \frac{jk_\circ\cos\theta}{2\pi}\frac{e^{-jk_\circ r}}{r}\widetilde{G}_\theta^M(k_{xs},k_{ys})\sum_{j\in A}\cdot E_j\left\{-\widetilde{T}_{xj}^*(k_{xs},k_{ys})\sin\phi+\widetilde{T}_{yj}^*(k_{xs},k_{ys})\cos\phi\right\} \tag{11}$$

$$E_\phi = \frac{jk_\circ\cos\theta}{2\pi}\frac{e^{-jk_\circ r}}{r}\widetilde{G}_\phi^M(k_{xs},k_{ys})\sum_{j\in A}\cdot E_j\left\{\widetilde{T}_{xj}^*(k_{xs},k_{ys})\cos\phi+\widetilde{T}_{yj}^*(k_{xs},k_{ys})\sin\phi\right\} \tag{12}$$

where A is a triangle in the aperture. Knowing the far-zone fields, antenna characteristics such as RCS, directivity, gain, and efficiency can be calculated.

B. Magnetized Ferrites

A magnetized ferrite slab can support two different type of waves known as the *ordinary* and the *extraordinary* waves [7], [15]. The ordinary wave is simply the same as the wave that would exist inside a pure dielectric material and polarized perpendicular to the direction of the bias field. The propagation characteristics of this type of wave are totally unaffected by the magnetization of the ferrite. On the other hand, the extraordinary wave is polarized along the direction of the bias field, therefore, it is strongly affected by the magnetization. The propagation constant of the extraordinary wave inside the ferrite is given by [15], [16]

$$\beta_e = \omega\sqrt{\epsilon\mu_{\text{eff}}} \tag{13}$$

with

$$\mu_{\text{eff}} = \frac{\mu^2-\kappa^2}{\mu} \tag{14}$$

$$\mu = \mu_\circ \left(1 + \frac{\omega_\circ \omega_m}{\omega_\circ^2 - \omega^2}\right) \tag{15}$$

$$\kappa = \mu_\circ \left(\frac{\omega \omega_m}{\omega_\circ^2 - \omega^2}\right) \tag{16}$$

where $\omega_\circ = \gamma[H_\circ + j(\Delta H/2)]$ and $\omega_m = \gamma(4\pi M_s)/\mu_\circ$; γ is the gyromagnetic ratio given by 1.76×10^7 rad/(s · Oe). In these expressions, the internal to the ferrite sample magnetic field is denoted as $H_\circ$, the linewidth as ΔH, and the saturation magnetization as $4\pi M_s$. In general, the ordinary and extraordinary waves are coupled. However, depending on the polarization of the excitation field and the direction of the bias field, the propagating wave inside the ferrite might exhibit properties of either the extraordinary or the ordinary wave; sometimes a combination of the two waves. Also, from (14) it is apparent that the effective permeability μ_{eff} may become negative for certain values of ω, $\omega_\circ$, and ω_m. In such a case, the propagation constant becomes imaginary and, therefore, the wave attenuates rapidly (evanescent wave) as it propagates through the ferrite slab. This phenomenon is usually referred to as the *cutoff* state of the ferrite. The frequency range where μ_{eff} is negative is given by

$$\sqrt{\omega_\circ(\omega_\circ + \omega_m)} \le \omega \le \omega_\circ + \omega_m. \tag{17}$$

The permeability of a magnetized ferrite is numerically modeled using a tensor notation. Depending on the direction of the bias field, the structure of the tensor varies. For example, when the ferrite is magnetized in the z direction, the complex permeability tensor is expressed as

$$[\mu] = \begin{bmatrix} \mu & -j\kappa, & 0 \\ j\kappa, & \mu & 0 \\ 0 & 0, & \mu_\circ \end{bmatrix} \tag{18}$$

where μ and κ are explicitly given in (15) and (16). In case the direction of magnetization is along the x or y axis, the ferrite permeability tensor has to be rotated by 90°.

C. Demagnetization Effects

When an arbitrary piece of ferrite is placed in a uniform magnetic field, the magnetic dipoles inside the material tend to align themselves along the direction of the bias field. Thus, the net field inside the ferrite (which is the one that correctly determines the elements of the permeability tensor) is a contribution of the external field and the field produced by the magnetic dipoles known as the "demagnetizing field." It is referred to as the demagnetizing field because it acts in a direction opposite to the bias. In general, the field inside the ferrite is nonuniform and different from the externally bias field. Also, it depends on the intensity of the bias field, the shape of the ferrite sample, and its orientation with respect to the bias direction. Thus, the internal field is usually written as

$$\mathbf{H}_o = \mathbf{H}_e - \bar{\bar{N}}\mathbf{M} \tag{19}$$

where $\bar{\bar{N}}$ is a 3×3 matrix denoted as the demagnetizing factor, and $\mathbf{M}$ is the magnetization vector. In this paper, the demagnetizing factor is considered a scalar number ranging between zero and one; its definition assumes that the demagnetizing field is in the opposite direction of the bias field; that is

$$H_\circ = H_e - N(4\pi M_s)/\mu_\circ. \tag{20}$$

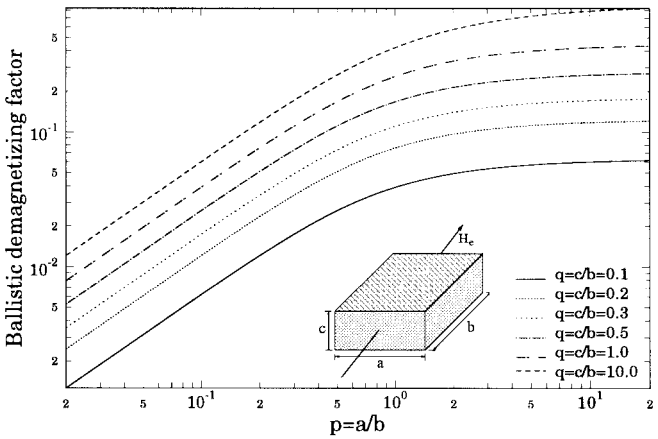

Fig. 2. The ballistic demagnetizing factor of a rectangular prism in a uniform bias field.

Although the derivation of the demagnetizing factor for a thin infinite ferrite layer is straightforward and well documented in various textbooks [15], the same analytical process becomes quite cumbersome for generic shapes. Joseph and Schlömann [17] derived closed-form expressions for the demagnetizing factor of a rectangular ferrite prism in a uniform dc magnetic field. Their approach is based on solving the Maxwell's equations for a magnetostatic problem.

According to Joseph [18], in most situations one is interested not in the local variations of the demagnetizing factor inside the ferrite volume, but rather in how the sample responds in some average sense to the externally bias field. Thus, one may suggest two different definitions of the demagnetizing factor: the *ballistic* and the *magnetometric*. The ballistic demagnetizing factor is defined, according to [18], as the average of the spatially varying demagnetizing factor in a plane perpendicular to the direction of the applied field and midway between the endfaces of the sample. The magnetometric demagnetizing factor is defined, according to [18], as the average of the spatially varying demagnetizing factor over the volume of the sample. In this paper, the ballistic demagnetizing factor is adopted. The corresponding expressions for a rectangular prism in a uniform magnetic field can be found in [19].

The ballistic demagnetizing factor is plotted in Fig. 2 on a logarithmic scale for various values of p $(= a/b)$ and q $(= c/b)$. For a constant value of q, the ballistic demagnetizing factor increases with increasing p until it eventually reaches a maximum. This maximum corresponds to the case when one of the horizontal dimensions, in this case a, extends to infinity. As q begins to increase, which is equivalent to increasing the vertical dimension (c), the entire graph shifts upward. In that case, the ballistic demagnetizing factor approaches unity.

Based on this magnetostatic formulation, an appropriate demagnetizing factor will be estimated in this paper in order to compute, in an average sense, the magnetic field inside a

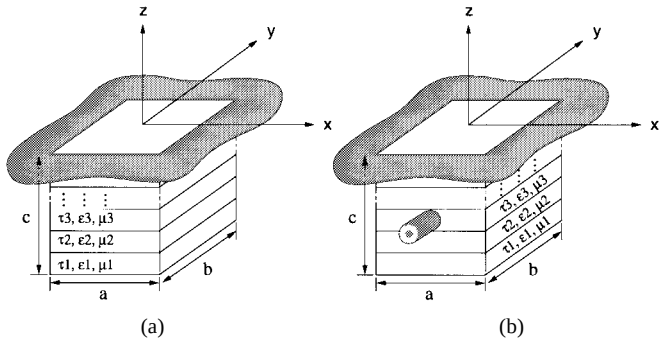

Fig. 3. A multilayer ferrite-loaded CBS mounted on an infinite ground plane. (a) Scatterer (without probe). (b) Antenna (with probe).

rectangular ferrite prism. Rectangular ferrite layers with finite thickness are used in this study as loading materials for CBS antennas.

III. Results

A. Scattering

The FEM, which was fully hybridized with the spectral and spatial-domain MoM, was implemented for the analysis of CBS antennas loaded with magnetized ferrites. The accuracy and validity of the code was first evaluated for numerous dielectric-loaded CBS antennas and later for ferrite-loaded CBS antennas.

Consider the multiferrite layer CBS shown in Fig. 3(a). This geometry was originally designed and analyzed by Kokotoff [10] using both experiments and moment method simulations. The cavity volume is partitioned horizontally into five rectangular sections. Each section is filled with either dielectric or ferrite material. The material numbering starts in ascending order from bottom to top. The dimensions of the cavity are $a = 2$ in, $b = 2$ in and $c = 2$ in. The infinite ground plane is treated as a perfect electric conductor without overlay. Material parameters and other dimensions are tabulated in Table I. The monostatic RCS is calculated versus frequency for a plane wave at normal incidence. The ferrite samples are magnetized in the y direction with an internal magnetic field of $H_\circ = 400$ Oe. The predicted data ($\sigma_{\phi\phi}$) using the present formulation are compared with data obtained by Kokotoff using pure MoM. As depicted in Fig. 4, the two data sets are in excellent agreement. Kokotoff's data, shown as markers in this figure, are only plotted up to a frequency of 850 MHz because the approach implemented in [10] becomes quite unstable at higher frequencies, possibly due to numerical errors. This can be thought of as another advantage of using FEM instead of MoM to solve for the fields inside the ferrite-loaded cavity.

The ability to effectively tune the ferrite-loaded CBS, shown in Fig. 3(a), is illustrated by varying the internal magnetic field $H_\circ$. The strength of the magnetic field was constantly increased from 400 to 700 Oe. As shown in Fig. 5, the resonant frequency of the structure shifts to a higher value as $H_\circ$ increases. This frequency tuning is attributed to the *extraordinary* properties of the ferrite that are controlled by the entries of the permeability tensor. By plotting the effective

TABLE I
Geometry and Material Specifications of the Scatterer

Material # (i)	Thickness, τ_i (cm)	Permittivity, ϵ_{r_i}	Permeability, μ_{r_i}
1	1.065	1	1
2	0.762	13.9	Ferrite: $\mu_r = 1$, $\Delta H = 5$ Oe, $4\pi M_s = 800$ Oe
3	0.737	2.2	1
4	1.790	13.9	Ferrite: $\mu_r = 1$, $\Delta H = 5$ Oe, $4\pi M_s = 800$ Oe
5	0.726	2.2	1

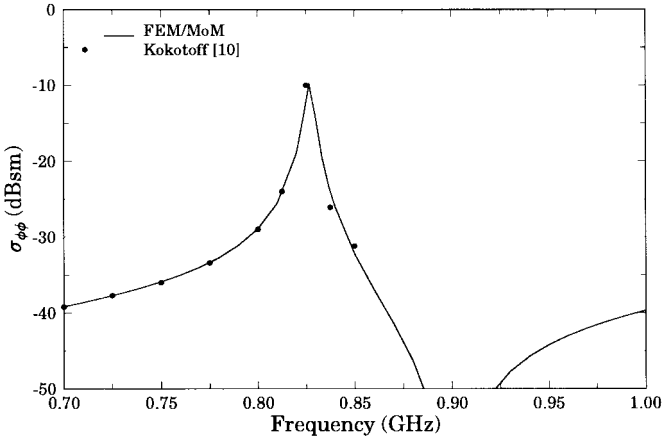

Fig. 4. Monostatic RCS of a ferrite-loaded CBS (scatterer) versus frequency at normal incidence ($\theta_i = \phi_i = 0^\circ$). The cavity is loaded with layers of ferrite that are magnetized along the y direction using an internal magnetic field $H_\circ = 400$ Oe.

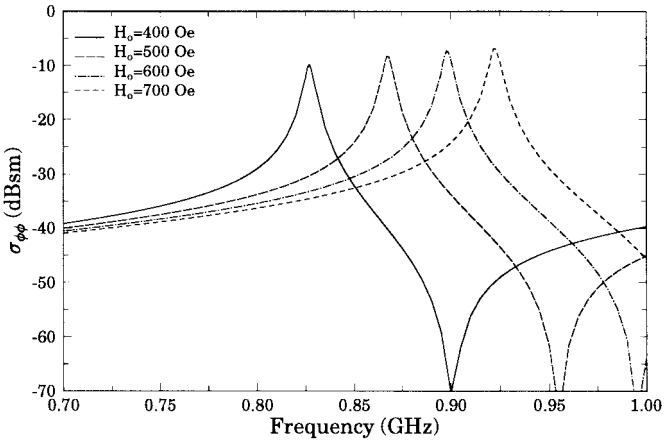

Fig. 5. Frequency tuning by varying the internal magnetic field ($H_\circ$) of ferrite layers inside the scatterer. The magnetization is oriented along the y direction.

permeability for the extraordinary wave inside a homogeneous ferrite medium, one can identify three regions of interest: the *low-frequency region*, the *resonant frequency* region, and the *high-frequency region*. In the low-frequency region, which is the region of interest in this study, the effective permeability shifts down to lower values as $H_\circ$ increases. This means that the effective aperture of the antenna becomes electrically smaller thereby shifting the magnetostatic resonance to higher frequencies. In the high-frequency region, where most microstrip dipole and patch antennas operate, a similar effect is observed. By increasing $H_\circ$, the effective permeability begins

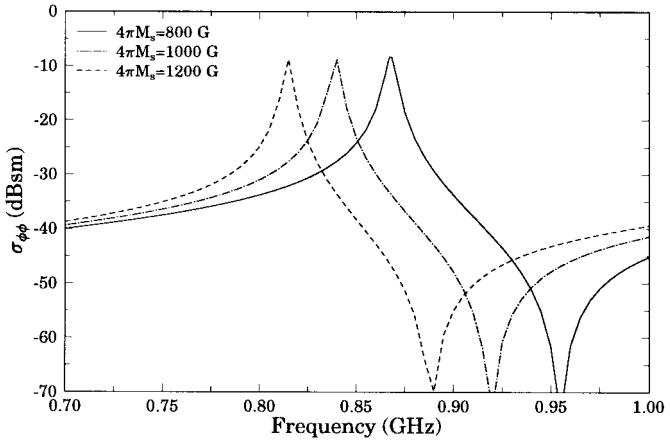

Fig. 6. The effect of saturation magnetization ($4\pi M_s$) on the monostatic RCS of a ferrite-loaded CBS (scatterer) at normal incidence. The magnetization is oriented along the y direction.

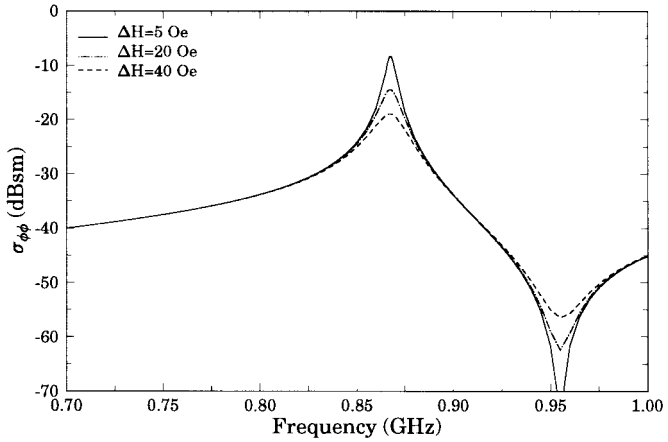

Fig. 7. The effect of linewidth (ΔH) on the monostatic RCS of a ferrite-loaded CBS (scatterer) at normal incidence. The magnetization is oriented along the y direction.

to decrease; therefore, the magnetostatic resonance shifts to a higher frequency. In the resonant frequency region, the effective permeability increases to extreme values before it actually becomes negative, therefore suggesting a highly lossy ferrite. When lossy, the ferrite can be used as an absorber. This property of ferrites finds numerous applications in RCS reduction and switchable antennas.

Besides varying the bias magnetic field H_o, the saturation magnetization $4\pi M_s$ is also varied while monitoring the resonant frequency of the scatterer. As $4\pi M_s$ increases from 800 to 1200 G (see Fig. 6), the first resonance starts to shift to a lower frequency. Increasing $4\pi M_s$ results in a larger effective permeability, which means a lower resonant frequency for the magnetostatic mode. This is true only in the low-frequency region; in the high-frequency region, the effect of increasing $4\pi M_s$ is reversed. A higher value for $4\pi M_s$ results in a lower effective permeability; however, the amount of shift in the resonant frequency of the antenna is almost negligible since the effective μ_r asymptotically approaches unity.

The RCS of a multilayer ferrite-loaded CBS also depends on the linewidth ΔH of the ferrite. The effect of ΔH on the magnetostatic-mode resonance is illustrated in Fig. 7 for the ϕ polarization. The linewidth is often conceptualized as the lossy term of the ferrite. By increasing the linewidth, the resonant peak of the magnetostatic mode is significantly reduced due to energy dissipation inside the ferrite. However, the resonant frequency remains unaffected.

B. Radiation

Consider a similar CBS shown in Fig. 3(b). The structure is now treated as a radiator rather than as a scatterer. It is excited horizontally using a y directed cylindrical probe with diameter 0.0624 in and length 1.75 in. The probe is soldered to the inner conductor of a 50-Ω coaxial cable centered at the midpoint of the cavity's sidewall. By simulating an empty cavity, it was observed that this specific antenna provides a fairly good match at a frequency around 4 GHz. However, the objective of this study is to design a tunable CBS antenna that operates within the UHF band. With this goal in mind, four layers of

TABLE II
GEOMETRY AND MATERIAL SPECIFICATIONS OF THE ANTENNA

Material # (i)	Thickness, τ_i (cm)	Permittivity, ϵ_{r_i}	Permeability, μ_{r_i}
1	0.635	2.2	1
2	0.762	13.9	Ferrite: $\mu_r = 1$, $\Delta H = 9$ Oe, $4\pi M_s = 800$ Oe
3	1.974	1	1
4	1.790	13.9	Ferrite: $\mu_r = 1$, $\Delta H = 9$ Oe, $4\pi M_s = 800$ Oe

ferrite and dielectric material are placed horizontally inside the cavity. The dimensions and material specifications are depicted in Table II. The inserted ferrite layers are magnetized using a pair of permanent magnets; one magnet on each side of the CBS antenna. The externally bias field is oriented along the length of the probe. To be able to simulate this antenna using numerical techniques, the strength of the actual magnetic field inside the ferrite slabs must be known precisely. Its value is found by subtracting the demagnetizing field, which exists inside the rectangular ferrite sample, from the externally bias field. The appropriate demagnetizing factor can be estimated based on the magnetostatic model briefly presented in the previous section. The externally bias field was measured using a Gaussmeter at various discrete points inside the cavity. The dielectric and ferrite layers had been removed from the cavity beforehand. Two separate measurements were performed: the first using one pair of magnets and the second using two pairs of magnets. Three-dimensional plots of the magnetic field distribution inside the empty cavity are shown in Fig. 8(a) and (b) for the cases of one and two pairs of magnets, respectively. The measurement data were curve-fitted using cubic splines. As expected, the field distribution exhibits some fringing effects. This phenomenon is primarily due to the cavity walls and the finite dimensions of the magnets. Note that the measured field inside the cavity is not the same as the field inside the ferrite. To compute the internal field, the demagnetizing field has to be estimated first based on the actual dimensions of the ferrite sample. However, in order for someone to use the results depicted in Fig. 2, the externally bias field has to be uniform. The assumption of a uniform bias field was introduced in the numerical model by averaging

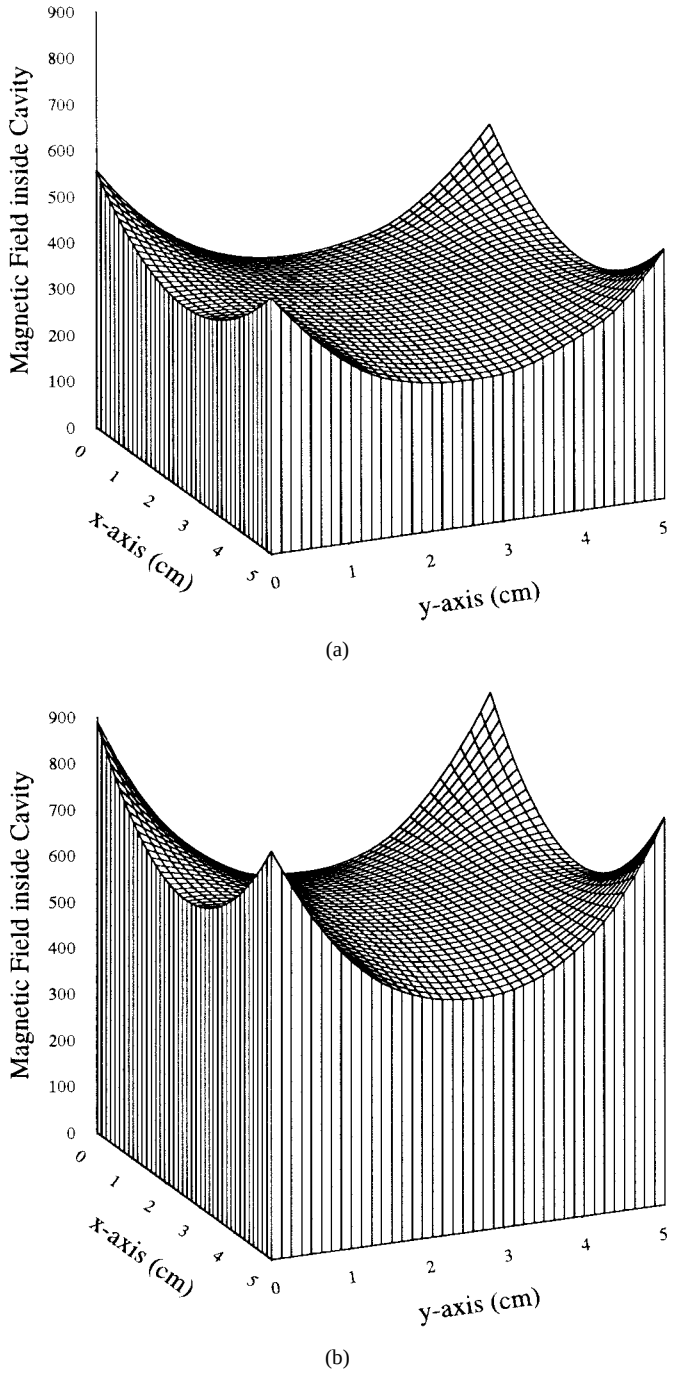

Fig. 8. Measured magnetic field distribution inside the air-filled cavity. The magnets are placed on each side of the cavity in such a way that the magnetization is oriented along the y direction. (a) Single pair of magnets. (b) Two pairs of magnets.

the field distribution shown in Fig. 8(a) and (b). A similar type of averaging was also introduced by Joseph [18], [19] in order to derive the expressions for the ballistic demagnetizing factor used in this study. For the two cases of magnetization, i.e., using one pair and two pairs of magnets, the averaged uniform magnetic field was found to be approximately 375 and 580 Oe, respectively.

The demagnetizing factor, as noted in the previous section, is determined by the actual dimensions of the ferrite layers as well as the orientation of the bias field. Specifically, there are two rectangular ferrite layers inside the cavity. Their dimensions are 5.08 $\times$ 5.08 $\times$ 1.79 cm and 5.08 $\times$ 5.08 $\times$ 0.762 cm. Due to their close proximity, the two samples are treated as a single ferrite sample with effective dimensions of 5.08 $\times$ 5.08 $\times$ 2.552 cm. The orientation of the bias field is along the y direction. Using Fig. 2, the corresponding demagnetizing factor is found to be approximately 0.17. Thus, for the two cases of magnetization, the uniform magnetic field (in an average sense) inside the ferrite is given by

$$H_\circ \simeq H_e - N \cdot (4\pi M_s)/\mu_\circ = 375 - 0.17 \cdot 800 = 239 \text{ Oe} \quad \text{for one pair of magnets} \tag{21}$$

$$H_\circ \simeq H_e - N \cdot (4\pi M_s)/\mu_\circ = 580 - 0.17 \cdot 800 = 444 \text{ Oe} \quad \text{for two pairs of magnets.} \tag{22}$$

It is important to emphasize here that these estimated values of the internal magnetic field are subject to tolerances related to experimental error and minor assumptions introduced in the model. Experimental errors were introduced in the analysis during the process of measuring the magnetic field inside the cavity. Besides tolerances associated with the Gaussmeter and other instruments, it was observed during the experiment that the field inside the cavity was quite sensitive to the position of the magnets. A slight misalignment of the magnets would result in a minor shift in the resonant frequency. Thus, extra precautions were taken during the experiment to ensure that the magnets were perfectly aligned and fixed to their position.

Using the above estimates for the internal field of the ferrites, the present formulation was implemented to predict the input impedance of the ferrite-loaded CBS antenna shown in Fig. 3(b). To the knowledge of the authors, this is the first paper to present comparisons between measurements and predictions of ferrite-tunable antennas. A comparison depicting the input impedance versus frequency, when the antenna is magnetized in the y direction using a single pair of magnets, is illustrated in Fig. 9. An internal magnetic field of $H_\circ = 238$ Oe was used for the simulation. The agreement between measurements and prediction is very good. Note that the existence of the indicated resonance is due to the presence of an externally bias field. If the magnets are removed from the sidewalls of the cavity, the magnetostatic resonance totally disappears.

The main objective of this project, of course, was to achieve frequency-tuning capabilities within the UHF band. Thus, another pair of magnets was placed on top of the old ones. An internal magnetic field of $H_\circ = 445$ Oe was used for the simulation. The comparison between measurements and predictions is shown in the same figure as the previous case (Fig. 9). The agreement between the two data sets is excellent. The hybrid FEM/MoM formulation predicts correctly not only the precise frequency shift of the magnetostatic resonance, but also the amplitude and shape of the input impedance. Also, comparing the two simulations in Fig. 9, it is interesting to observe that an increase of 200 Oe in the externally bias field causes the resonant frequency of the magnetostatic mode to shift by as much as 120 MHz. When the internal magnetic field $H_\circ$ increases to 1000 Oe, the resonant frequency shifts by 220 MHz, whereas when $H_\circ$ increases to 2000 Oe the resonant

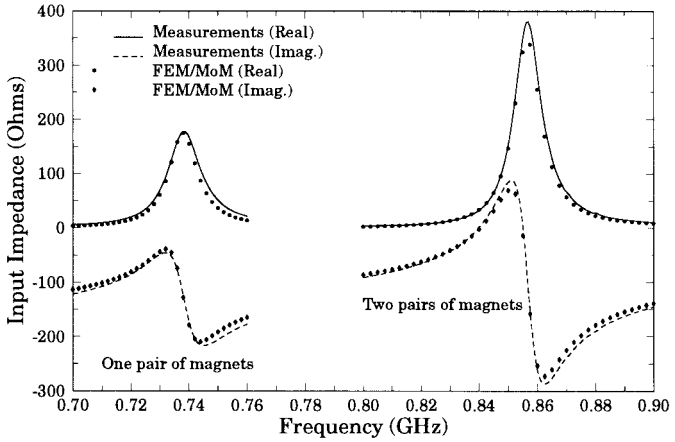

Fig. 9. Predicted and measured input impedance versus frequency of the ferrite-loaded CBS antenna. One pair of magnets corresponds to $H_\circ = 238$ Oe; two pairs of magnets correspond to $H_\circ = 445$ Oe.

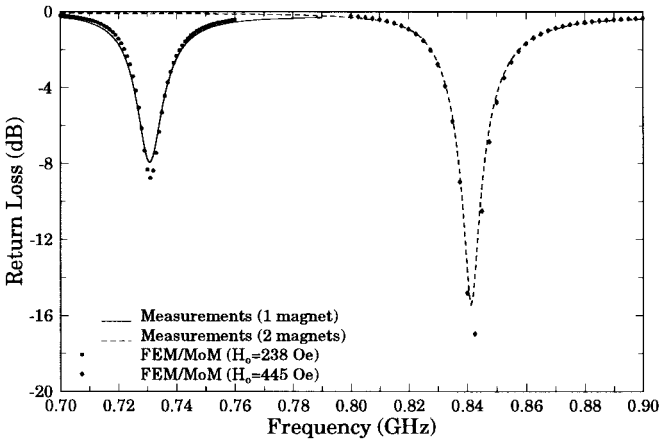

Fig. 11. Predicted and measured return loss versus frequency of the ferrite-loaded CBS antenna using one and two pairs of magnets ($H_\circ = 238$, 445 Oe).

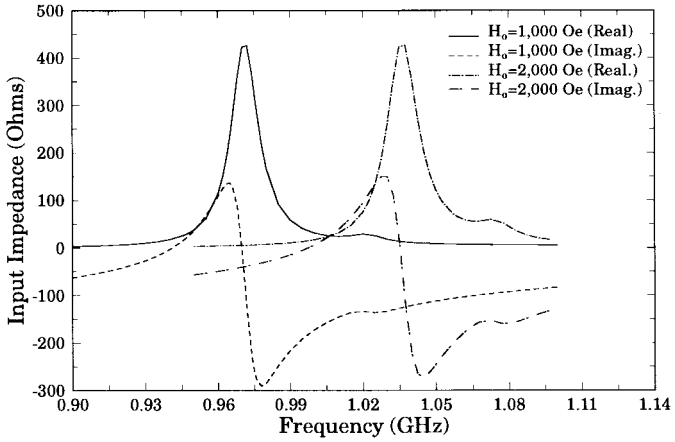

Fig. 10. Predicted input impedance versus frequency of the ferrite-loaded CBS antenna using various biasing fields.

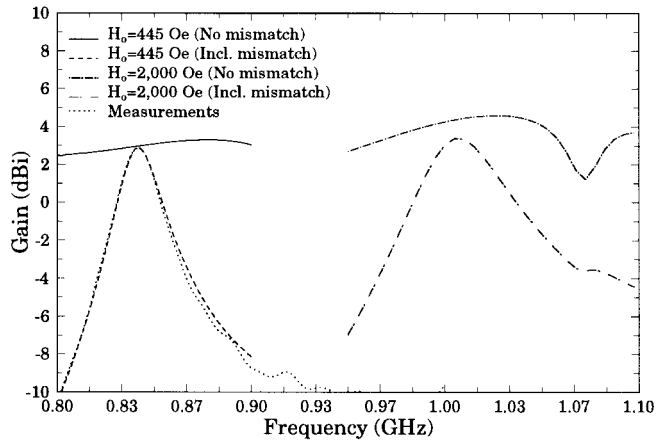

Fig. 12. Predicted and measured gain versus frequency of the ferrite-loaded CBS antenna using various biasing fields (ϕ polarization).

frequency shifts by almost 300 MHz. The input impedance versus frequency for the last two cases of magnetization is illustrated in Fig. 10. Note that the percentage change in frequency tuning decreases substantially with increasing $H_\circ$. From these figures, it is apparent that the ferrite-loaded CBS antenna is tunable between 700 to 1100 MHz. Assuming the center frequency of operation is 900 MHz, the percentage tuning of the antenna is about 45%. The tuning mechanism can be achieved quite effectively by placing an electromagnet in the direction of the probe.

The return loss of the antenna for the first two cases of magnetization, i.e., $H_\circ = 238$ Oe and $H_\circ = 445$ Oe, is compared with measurements in Fig. 11. Again, the agreement between the two data sets is excellent. Note that for the lower resonance, the return loss is -9 dB, whereas for the higher resonance, the return loss improves to -17 dB. The coaxial cable was chosen to have a 50-Ω characteristic impedance. For better return loss, a custom made coaxial cable is probably a good choice. Of course, antenna design optimization is always another option.

Besides input impedance and return loss, gain is also an important measure to calculate. In Fig. 12, the gain (ϕ polarization) is shown for two different magnetizations: $H_\circ = 445$ Oe and $H_\circ = 2000$ Oe. One set of plots represents the gain including the mismatch loss and the other set of plots represents the gain without the mismatch loss. Obviously, when the mismatch loss is accounted for the gain is maximum at the resonant frequency of the antenna. This maximum was found to be 2.9 dBi at 842.5 MHz and 3.4 dBi at 1010 MHz. By neglecting the mismatch loss, the efficiency of the antenna at a frequency of 842.5 MHz and 1010 MHz is 60% and 90%, respectively. This means that more energy is dissipated inside the ferrite when the magnetization is 445 Oe rather than 2000 Oe. Gain measurements are shown in the graph only for the case of magnetizing the antenna using two pairs of magnets. The agreement between measurements and predictions is excellent. The small discrepancies observed are attributed to diffractions from the edges of the finite ground plane (9 ft long in the y direction). Note also that gain improvement can be achieved at the cost of bandwidth; however, bandwidth is not a major issue in tunable antennas. One way to improve gain is by placing multiple superstrates on top of the infi-

nite ground plane [21], [22]. An optimization code can be used to select optimum values for thickness and material parameters.

IV. Conclusions

A hybrid FEM/MoM formulation was presented for the analysis of a ferrite-tuned cavity-backed slot antenna with possible dielectric overlay. The antenna under investigation is tunable within the UHF band through altering the externally bias magnetic field. Scattering and radiation characteristics were calculated and compared with measurements and data from other independent sources. The agreement between predicted and comparison data was excellent. It was also illustrated in this paper that tuning capabilities up to 45% can be achieved at a center frequency of 900 MHz. The antenna has an absolute gain of 3 dBi and a directivity of 5 dBi. Depending on the specific application, design optimization of this antenna can be used to improve certain radiation characteristics. This topic is currently under investigation.

References

[1] H. L. Glass, "Ferrite films for microwave and millimeter wave devices," *Proc. IEEE*, vol. 76, pp. 151–158, Feb. 1988.

[2] D. M. Pozar and V. Sanchez, "Magnetic tuning of a microstrip antenna on a ferrite substrate," *Electron. Lett.*, vol. 24, pp. 729–731, June 1988.

[3] D. M. Pozar, "Radar cross-section of a microstrip antenna on normally biased ferrite substrate," *Electron. Lett.*, vol. 25, pp. 1079–1080, Aug. 1989.

[4] ———, "Radiation and scattering characteristics of microstrip antennas on normally biased ferrite substrates," *IEEE Trans. Antennas Propagat.*, vol. 40, pp. 1084–1092, Sept. 1992.

[5] ———, "Correction to radiation and scattering characteristics of microstrip antennas on normally biased ferrite substrates," *IEEE Trans. Antennas Propagat.*, vol. 42, pp. 122–123, Jan. 1994.

[6] H.-Y. Yang, J. A. Castaneda, and N. D. Alexópoulos, "The RCS of a microstrip patch on an arbitrary biased ferrite substrate," *IEEE Trans. Antennas Propagat.*, vol. 41, pp. 1610–1614, Dec. 1993.

[7] H.-Y. Yang, "Characteristics of switchable ferrite microstrip antennas," *IEEE Trans. Antennas Propagat.*, vol. 44, pp. 1127–1132, Aug. 1996.

[8] B. Lee and F. J. Harackiewicz, "The RCS of a microstrip antenna on an in-plane biased ferrite substrate," *IEEE Trans. Antennas Propagat.*, vol. 44, pp. 208–211, Feb. 1996.

[9] N. E. Buris, T. B. Funk, and R. S. Silverstein, "Dipole arrays printed on ferrite substrates," *IEEE Trans. Antennas Propagat.*, vol. 41, pp. 165–175, Feb. 1993.

[10] D. Kokotoff, "Full-wave analysis of a ferrite-tuned cavity-backed slot antenna," Ph.D. dissertation, Arizona State Univ., Tempe, AZ, 1995.

[11] S. M. Rao, D. R. Wilton, and A. W. Glisson, "Electromagnetic scattering by surfaces of arbitrary shape," *IEEE Trans. Antennas Propagat.*, vol. AP-30, pp. 409–418, May 1982.

[12] K. McInturff and P. S. Simon, "The Fourier transform of linearly varying functions with polygonal support," *IEEE Trans. Antennas Propagat.*, vol. 39, pp. 1441–1443, Sept. 1991.

[13] A. Polycarpou, "Finite-element analysis of microwave passive devices and ferrite-tuned antennas," Ph.D. dissertation, Arizona State Univ., Tempe, AZ, 1998.

[14] J. T. Aberle, "Spectral domain method of moments," personal notes, June 1994.

[15] D. M. Pozar, *Microwave Engineering.* Reading, MA: Addison-Wesley, 1990.

[16] B. Lax and K. J. Button, *Microwave Ferrites and Ferrimagnetics.* New York: McGraw-Hill, 1962.

[17] R. I. Joseph and E. Schlömann, "Demagnetizing field in nonellipsoidal bodies," *J. Appl. Phys.*, vol. 36, no. 5, pp. 1579–1593, May 1965.

[18] R. I. Joseph, "Ballistic demagnetizing factors in uniformly magnetized cylinders," *J. Appl. Phys.*, vol. 38, no. 13, pp. 4639–4643, Dec. 1966.

[19] ———, "Ballistic demagnetizing factors in uniformly magnetized rectangular prisms," *J. Appl. Phys.*, vol. 38, pp. 2405–2406, 1967.

[20] A. C. Polycarpou, M. R. Lyons, J. T. Aberle, and C. A. Balanis, "Analysis of arbitrary shaped cavity-backed patch antennas using a hybridization of the finite element and spectral domain methods," in *IEEE Antennas Propagat. Soc. Int. Symp.*, Baltimore, MD, July 1996, pp. 130–133.

[21] X.-H. Shen, G. A. E. Vandenbosch, and V. Antoine, "Study of gain enhancement method for microstrip antennas using moment method," *IEEE Trans. Antennas Propagat.*, vol. 43, pp. 227–231, Mar. 1995.

[22] H.-Y. Yang and N. G. Alexopoulos, "Gain enhancement methods for printed circuit antennas through multiple superstrates," *IEEE Trans. Antennas Propagat.*, vol. AP-35, pp. 860–863, July 1987.

Anastasis C. Polycarpou (S'92) was born in Nicosia, Cyprus, on October 1967. He received the B.S. (electrical engineering—*summa cum laude*), M.S., and Ph.D. degrees, all from Arizona State University (ASU), Tempe in 1992, 1994, and 1998, respectively.

In the fall of 1992, he joined the Telecommunications Research Center (TRC) at ASU as a Graduate Research Assistant, where he worked on a variety of numerical techniques with applications to scattering, radiation, and microwave circuit/packaging characterization. He is now a Faculty Research Associate at ASU. His current research interests include the finite-element method as applied to complex electromagnetic problems.

Constantine A. Balanis (S'62–M'68–SM'74–F'86) received the B.S.E.E. degree from Virginia Tech, Blacksburg, VA, in 1964, the M.E.E. degree from the University of Virginia, Charlottesville, VA, in 1966, and the Ph.D. degree in electrical engineering from Ohio State University, Columbus, OH, in 1969.

From 1964 to 1970, he was with NASA Langley Research Center, Hampton, VA, and from 1970 to 1983 he was with the Department of Electrical Engineering, West Virginia University, Morgantown, WVA. Since 1983, he has been with the Department of Electrical Engineering, Arizona State University, Tempe, where he is now Regent's Professor and Director of the Telecommunications Research Center. He has served as the Associate Editor of the *Institute of Electrical Engineers Transactions on Antennas and Propagation* (1974–1977), *Institute of Electrical Engineers Transactions on Geoscience and Remote Sensing* (1981–1984) and Editor of the *Newsletter for the IEEE Geoscience and Remote Sensing Society* (1982–1983). He is the author of *Antenna Theory: Analysis and Design* (New York: Wiley, 1997; 1982) and *Advanced Engineering Electromagnetics* (New York: Wiley, 1989). His research interests are in low- and high-frequency computational methods for antennas, scattering, and penetration, transient analysis, control of coupling and reduction of pulse distortion in interconnects for monolithic microwave and millimeter-wave circuits, modeling of electronic packages for microwave, millimeter-wave, and high-speed high-density integrated circuits, and multipath propagation.

Dr. Balanis received the 1992 Special Professionalism Award from the IEEE Phoenix Section, the 1989 IEEE Region 6 Individual Achievement Award, the 1996 Arizona State University Outstanding Graduate Mentor Award, and the 1987–1988 Graduate Teaching Excellence Award, School of Engineering, Arizona State University. He is a member of ASEE, Sigma Xi, Electromagnetics Academy, Tau Beta Pi, Eta Kappa Nu, and Phi Kappa Phi. He was Second Vice-President (1984) and member of the Administrative Committee (1984–1985) of the IEEE Geoscience and Remote Sensing Society, Chairman of the Distinguished Lecturer Program of the IEEE Antennas and Propagation Society (1988–1991), and member of the AdCom (1992–1995, 1997–1999) of the IEEE Antennas and Propagation Society.

James T. Aberle (S'81–M'89–SM'92) received the B.S. and M.S. degrees in electrical engineering from the Polytechnic Institute of New York (now Polytechnic University), Brooklyn, NY, in 1982 and 1985, respectively, and the Ph.D. degree in electrical engineering from the University of Massachusetts, Amherst, in 1989.

From 1982 to 1985, he was employed by Hazeline Corporation, Greenlawn, NY, where he worked on the development of wide-band phased-array antennas. He was a Graduate Research Assistant at the University of Massachusetts, Amherst, from 1985 to 1989, where he developed and validated computer models for printed antennas. He has been a Faculty Member at Arizona State University since 1989. During the summer of 1993, he was a NASA/ASEE Summer Faculty Fellow at NASA Langley Research Center, Hampton, VA. Currently, he is an Associate Professor at Arizona State University, Tempe. His research interests include the modeling of complex electromagnetic phenomena. During his sabbatical from 1997 to 1998, he was a Visiting Academic at the Royal Melbourne Institute of Technology in Melbourne, Victoria, Australia, and a Visiting Researcher at Atlantic Aerospace Electronics Corp., Greenbelt, MD.

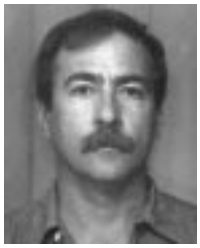

Craig R. Birtcher was born in Phoenix, AZ, on March 30, 1959. He received the B.S. and M.S. degrees, both in electrical engineering from Arizona State University, Tempe, in 1983 and 1992, respectively.

He has been at Arizona State University since 1987, where he is now an Associate Research Specialist in charge of the ElectroMagnetic Anechoic Chamber (EMAC) facility. His research interests include antenna and RCS measurement techniques, NF/FF techniques, and the measurement of electrical properties of solids.